Micromixing in a gas-liquid vortex reactor

Yi Ouyang, Manuel Nunez Manzano, Koenraad Beirnaert,

*Geraldine J. Heynderickx, Kevin M. Van Geem**

Ghent University, Laboratory for Chemical Technology, Technologiepark 125, 9052 Gent, Belgium.

*Corresponding author:

Kevin M. Van Geem

Laboratory for Chemical Technology, Ghent University, Belgium

Address: Technologiepark 125, B-9052 Ghent, Belgium

Tel. : +32 9 264 56 77 /Fax: +32 9 331 1759

Kevin.VanGeem@UGent.be

This article has been accepted for publication and undergone full peer review but has not been through the copyediting, typesetting, pagination and proofreading process which may lead to differences between this version and the Version of Record. Please cite this article as doi: 10.1002/aic.17064

Highlights

1. The Villermaux-Dushman protocol is used to quantify the micromixing efficiency of a gas-liquid vortex reactor.
2. The micromixing time of the GLVR is comparable to the highly efficient rotating packed bed and substantially better than a static mixer.
3. The energetic efficiency of the GLVR could be advantageous when using the GLVR as a mixer.

Keywords: Gas-liquid vortex reactor, Micromixing, Villermaux-Dushman protocol

Abstract:

The gas-liquid vortex reactor (GLVR) has substantial process intensification potential for multiphase processes. Essential in this respect is the micromixing efficiency, which is of great importance in fast reaction systems such as crystallization, polymerization and synthesis of nanomaterials. By creating a vortex flow and taking advantage of the centrifugal force field, the liquid micromixing process can be intensified in the GLVR. Results show that introducing a liquid into a gas-only vortex unit results in suppression of primary and secondary gas flow. The Villermaux-Dushman protocol is applied to study the effects of the gas flow rate, liquid flow rate and liquid viscosity based on a segregation index. Based on the incorporation model and reaction kinetics, the micromixing time of the GLVR is determined to be in the range of 10^{-4}~10^{-3} s, which is comparable to the highly efficient rotating packed bed and substantially better than a static mixer.

INTRODUCTION

Diffusive mixing on the Batchelor scale is commonly referred to as micromixing [1,2]. To achieve proper micromixing, two conditions must be met, firstly a region with high turbulent energy dissipation rate should be present and secondly the streams to be mixed must pass through this region [3,4]. As it is believed that both conditions will be met inside a gas-liquid vortex reactor (GLVR), see **Figure 1**, applying this technology for the intensification of micromixing controlled processes could be advantageous. In previous work [5], active and passive mixers were considered to be two basic mixer categories based on the criterion of external energy. Similar categories are defined in Liu et al.'s work [6] using the terms rotational and static mixing devices. Active mixers and rotational devices usually require external energy, such as mechanical rotation, ultrasound, microwave, etc. [7]. Adding an external energy source can improve the performance of the mixers or the devices, but at the same time increases the energy consumption. Until today vortex units have been mainly applied for gas-solid applications [8,9,18,10–17]. If the GLVR is used in micromixing applications, it is a type of unit that is situated between the active and passive mixers, or static and rotational reactors for two reasons: (1) a GLVR creates a gas-liquid system where the gas phase can be regarded as an external energy input; (2) a strong vortex (rotating) flow is created in the GLVR, but in a static geometry.

The design of the vortex reactor originates from the concept of rotating fluidized beds in a static geometry. One of the key parts of the vortex reactor is the tangential inlet slots positioned at the cylindrical circumferential wall of the reactor, which directs the gas flow and thus creates a vortex flow and centrifugal force field. In a GLVR, the gas momentum is transferred to the liquid in the reactor chamber, creating high turbulence and causing the rotation of the liquid. Preliminary experimental work was carried out by Kuzmin et al. in a bubbling system [19]. Results

show that the vortex unit can realize a large liquid specific surface area of 10^3 m^2/m^3 with a very high surface renewal rate in the range of 10-100 g centrifugal acceleration. This indicates that a region with a high energy dissipation rate per unit volume is created in the vortex chamber with the liquid stream passing through this region. In short, a high-gravity environment is created without mechanical rotation [19,20], which can realize considerable process intensification for mixing and mass transfer.

Obtaining a thorough understanding of the micromixing is especially important if the timescales for mixing are similar or larger than the characteristic timescales for reaction, causing the process to be (co-)governed by micromixing. Examples of process performance indicators affected by micromixing include local oversaturation (e.g. during crystallization), polydispersity (e.g. polymerization) and selectivity (e.g. organic synthesis) [5,21–25]. To target these process performance indicators, the micromixing performance of the reactors is a key factor [26,27].

In the present work, the effects of the liquid- and gas flowrates and the liquid viscosity on the micromixing efficiency will be investigated using the Villermaux-Dushman protocol. From these results, the characteristic timescale for micromixing [28] in the GLVR will be determined and compared to similar reactors and mixers.

MATERIALS AND METHODS

THE VILLERMAUX-DUSHMAN PROTOCOL

Approaches based on competing reaction system are widely used owing to their universal applicability, such as the azo reaction system [29,30] and the acid-base neutralization and alkaline hydrolysis of ethyl monochloroacetate system [31]. In particular, the iodide-iodate reaction system, also known as the Villermaux-Dushman protocol [32,33] is a commonly used chemical

quantification method for micromixing. The protocol consists of two competitive parallel reactions. The first reaction consists of a neutralization for which theoretically a multitude of buffer solutions could be used. The second one, named the Dushman reaction, is the redox reaction of iodide (I^-) and iodate (IO_3^-) forming iodine (I_2). Originally, the boric acid buffer pair ($H_2BO_3^-/H_3BO_3$) is chosen. Iodide (I^-) and iodine (I_2) are present and the equilibrium reaction forming triiodide (I_3^-) should also be considered. The resulting set of reactions is displayed in R1, R2 and R3. R1 and R3 are considered to be quasi-instantaneous and the redox reaction R2 is considered to be fast.

Quasi-instantaneous $$H^+ + H_2BO_3^- \overset{k_1}{\rightarrow} H_3BO_3 \quad \text{(R1)}$$

Fast $$6H^+ + 5I^- + IO_3^- \overset{k_2}{\rightarrow} 3I_2 + 3H_2O \quad \text{(R2)}$$

Quasi-instantaneous $$I^- + I_2 \underset{k_4}{\overset{k_3}{\leftrightarrow}} I_3^- \quad \text{(R3)}$$

To achieve competition between reaction R1 and R2, an acid and a buffer stream are mixed. The acid stream contains the protons (H^+) and the buffer stream contains the deprotonated boric acid, the iodide-ions and iodate-ions. When the acid and buffer stream mix, competition occurs between R1 and R2 for the stoichiometrically deficient protons. As the neutralization R1 is much faster than the redox reaction R2, in case of perfect micromixing only reaction R1 will occur. However, if fresh materials of $H_2BO_3^-$ component cannot be timely supplied in local regions, i.e., under non-ideal micromixing conditions, the byproducts I_2 and I_3^- will be produced in those local regions due to an excessive amount of hydrogen ions. The competition between R1 and R2 is illustrated in **Figure 2**.

If R2 occurs due to imperfect micromixing, triiodide can be formed through R3. Triiodide can be quantified spectroscopically at 353 nm. Thus, the simple spectroscopic measurement of triiodide

indicates the micromixing intensity in the unit. The micromixing intensity is quantified by the segregation index (X_S) which is calculated from the triiodide concentration as described below. The iodide and iodine concentrations can be determined from the triiodide concentration by simultaneously solving the iodine mass balance (Eq. 1) and the equilibrium equation of R3 (Eq. 2). Note that the equilibrium constant of R3 has a temperature dependence, as shown in Eq. 3 [34].

$$[\mathrm{I}^-]_0 = [\mathrm{I}^-] + 5/3([\mathrm{I}_2] + [\mathrm{I}_3^-]) + [\mathrm{I}_3^-] \quad (1)$$

$$K_{eq} = \frac{[\mathrm{I}_3^-]}{[\mathrm{I}_2][\mathrm{I}^-]} \quad (2)$$

$$\log_{10}(K_{eq}) = \frac{555}{\mathrm{T}} + 7.355 - 2.575\log_{10}T \quad (3)$$

From Eqs. 1-3 and the ratio of the buffer stream to the acid stream (R), two intermediary parameters (Y and Y_{ST}) can be calculated. Y represents the percentage of protons (H^+) consumed by R2 while Y_{ST} represents the same percentage if no micromixing would have occurred (i.e. under total segregation). The calculation of Y and Y_{ST} are respectively shown in Eq. 4 and Eq. 5.

$$Y = \frac{2(R+1)([I_2]+[I_3^-])}{[H^+]_0} \quad (4)$$

$$Y_{ST} = \frac{6[IO_3^-]_0}{6[IO_3^-]_0+[H_2BO_3^-]_0} \quad (5)$$

The ratio of Y and Y_{ST} (Eq. 6) gives the segregation index (X_S) which can be interpreted as the amount of hydrogen consumed by the side reaction divided by the maximal amount of hydrogen that could be consumed by the side reaction. Therefore, with an X_S value of 0 perfect micromixing occurs (i.e. no side reaction) and a value of 1 means total segregation.

$$X_S = \frac{Y}{Y_{ST}} \quad (6)$$

During its history, multiple improvements to the Villermaux-Dushman protocol have been proposed. Regarding the kinetics of the Dushman reaction (i.e. R2) [35–37], the parameters proposed in 2000 by Guichardon et al. [32] have mostly been applied. Regarding the choice of the acid to provide the protons, perchloric acid is preferred over sulfuric acid due to the influence of the two-step dissociation of sulfuric acid [32,38,39]. Finally, regarding the buffer solution [40], a boric acid buffer is preferred over a phosphate buffer due to the wider concentration range in which the buffer is stable [41]. Compared to a phosphate buffer, it is more favorable when experimental results using this buffer are compared with literature data.

INCORPORATION MODEL

To compare the micromixing efficiency of the GLVR with other units, a characteristic timescale for micromixing is calculated using the incorporation model presented by Fournier et al. [28]. The general principle of the incorporation model is presented in **Figure 3**. Given the large stream ratio (i.e. buffer stream flowrate to acid stream flowrate), the incorporation model assumes the fluid elements of the acid stream to be dispersed in the buffer stream. The model assumes that the acid fluid elements are progressively invaded by the environment (i.e. the buffer stream), causing the former to grow in time. The characteristic timescale of incorporation is assumed to be equal to the micromixing time (t_m), and thus by calculating the timescale of incorporation an estimation for the micromixing time is made.

The growth of the reactional volume is modeled as shown in Eq. 7, in which V_2 is the instantaneous volume, $V_{2,0}$ is the initial volume and $g(t)$ is the growth function. If the incorporation flow is assumed to be proportional on the V_2, the exponential growth function shown in Eq. 8 is obtained. Note that it is assumed that all reactions are occurring within the growing reactional volume.

$$V_2 = V_{2,0} * g(t) \quad (7)$$

$$g(t) = \exp(t/t_m) \quad (8)$$

Within the volume (i.e. dispersed acid stream elements), the time dependency of the concentration of the species is given by Eq. 9, in which the subscript 10 denotes the surrounding fluid (i.e. buffer stream), C_j represents the concentration of species j, and R_j the net production rate of species R_j via R1, R2 and R3. The governing equation of the incorporation model describes the growth of the aggregate reactional volume and a dilution-reaction scheme [21]:

$$\frac{dC_j}{dt} = \left(C_{j,10} - C_j\right)\frac{1}{g}\frac{dg}{dt} + R_j \quad (9)$$

The kinetics of R1, R2 and R3 used in this work are shown in **Table 1**. Note that the rate coefficient of R2 is a function of the ionic strength (*I*).

To obtain the micromixing time (t_m), Eq. 7-9 and kinetics in **Table 1** are solved simultaneously for every component and for varying time using a stiff differential solver.

GAS-LIQUID VORTEX REACTOR

The experimental setup, containing a liquid feeding section, a gas feeding section and a reacting section is shown in **Figure 4**.

In the liquid feeding section, the buffer solution is stored in a metal drum (max. capacity 25 liters), the acid solution is stored in a glass bottle (max. capacity 2 liters). To ensure a constant suction pressure for the pumps, both containers are pressurized using compressed air up to 0.2 bar. From their containers, the liquids are pumped to the premixer using two high precision rotary pumps (Tuthill DGS.11). Their mass flows are controlled using Coriolis mass flow controllers (Bronkhorst CORI-FLOW™ M54) with a mass flow rate range of 0.1-10 kg/h.

Downstream of the pumps, 4 mm plastic tubing is used to transport the liquid streams. Approximately 5 cm before the reacting section backflow valves (Festo H-QS-4) are installed in both lines. In the gas feeding section air is fed via a compressor (Atlas Copco GA90VSD) and its flow is controlled by a thermal mass flow controller (Bronkhorst F-106 CI).

in view of the liquid premixing inlet of the GLVR used in this work. The central reactor chamber has a diameter (D_R) of 139 mm and a length (H) of 25 mm. Half of the GLVR top plate is transparent as an observation window. The outlet of the reactor chamber is a vertically downwards oriented curved orifice in the middle of the unit with a diameter (D_E) of 40 mm. To avoid gas maldistribution, the compressed air flow is first split into two gas streams and then distributed over 8 sides of an external octagonal jacket. 16 slots are formed by the opening between adjacent vanes. Each slot has a width of 1 mm and is 2.5° tangentially inclined with respect to the reactor chamber. As a result, the gas is evenly split into 16 streams, each corresponding to a gas inlet slot of the GLVR. The two liquid streams are premixed in a T-fitting (Festo QSMT 4) before entering the GLVR at a radial distance of 55 mm from the center with an angle of 45°. The premix length (L) is 20 mm. An absolute pressure sensor and a gauge pressure sensor are located at the external side of the octagonal jacket and the outlet, respectively. The main dimensions and the operational ranges of the gas and liquid flow used in these experiments are displayed in **Table 2**.

CHEMICALS

The reagents used to prepare the buffer solution are boric acid with a 99.5% purity, sodium hydroxide with a 98% purity, potassium iodate with a 99.5% purity and potassium iodide with a 99.5% purity (all purchased from Sigma-Aldrich, Belgium). A solution of 70% perchloric acid is

used to prepare the acid solution. The initial solution concentrations for the iodide–iodate reaction system are shown in **Table 3**. The buffer solution is prepared as follows: boric acid powder is firstly dissolved, and then dissolved sodium hydroxide is added into the boric acid solution. Next, the potassium iodide solution and the potassium iodate solution are added in that order. To study the effect of the liquid viscosity on the micromixing efficiency of the GLVR, varying amounts of glycerin can be added to the buffer solution.

EXPERIMENTAL PROCEDURE

To obtain reproducible results, a strict experimental procedure is necessary. Before each experiment, the liquid feeding lines are thoroughly purged. Thereafter the reactor is rinsed by feeding 2 L demineralized water with the gas flow at 90 Nm^3/hr. Subsequently, the acid and buffer streams are started with the gas flow on. For a fixed acid/buffer concentration, the reactor is run continuously while the conditions are discretely changed, starting with the experiment yielding the lowest absorbance value and ending with the experiment yielding the highest. After a condition is changed, two wait steps are introduced, a first step to obtain a steady gas flow and a second step of 1.5 minutes to obtain a steady state in the reactor. After the assumed steady state is reached, three samples (0.5 min sampling interval) are taken and the conditions are changed. All the experiments are conducted at room temperature.

The samples are collected, sealed and analyzed within 10 minutes via spectrophotometer (Cary® 50 UV-Vis Spectrophotometer, Varian). The triiodide concentration is measured at 353 nm. A calibration curve for triiodide is provided in the supporting information. All the error bars shown in the following figures are based on a 99% confidence interval.

RESULTS AND DISCUSSION

EFFECT OF THE ACID CONCENTRATION AND STREAM RATIO

The first step when utilizing the Villermaux-Dushman protocol is determining a proper acid concentration and buffer to acid stream ratio (R) [5]. The first reason why this step is important relates to the sensitivity of the segregation index (X_S). If the acid concentration and stream ratio are chosen poorly, it is possible that no variation in the segregation index may be observed when changing the operating conditions. The second reason is related to the measurement constraints of the UV-vis spectrophotometer. The obtained absorbance values should remain in the operating range of the spectrophotometer. Thus a combination of acid concentration and stream ratio needs to be found which allows variations in the segregation index and for which each datapoint lies within the spectrophotometer's operating range. Two constraints rest upon these combinations, the first one being the fact that for the Villermaux-Dushman protocol, a large stoichiometric deficit of protons is necessary. The second one is a large stream ratio should be used for the incorporation model (e.g. R>5).

Several combinations of acid concentrations and stream ratios were tested under varying gas flow rates, as shown in **Figure 6a** and **b.** The gas flowrate is selected as a variable operating parameter**. Figure 6a** shows the influence of acid concentration under a constant stream ratio. Better tendencies (i.e. the X_S value being sensitive the operating condition) can be noted for acid concentrations of 0.45 mol/L and 0.35 mol/L while using an acid concentration of 0.25 mol/L the sensitivity is relatively small. **Figure 6b** shows, for a fixed acid concentration, the influence of the acid/buffer ratio on the segregation index. The curves at ratios of 10 and 15 show quasi identical tendencies while at a ratio of 5 less variance of the segregation index is observable. Two factors are in fact compensating each other: for a fixed the acid concentration, (1) a higher

liquid ratio corresponds to a lower absolute molar amount of hydrogen ions, indicating a reduction of byproducts formation; (2) according to Eqs. 4-6, if other parameters are fixed, the calculated X_S value will increase with a higher R value. Therefore, the absorbances of the samples under the condition of R=10 are actually always higher than R=15. However, the calculated segregation index values are similar. All of the data points showed in **Figure 6a** and **b** are within the operating range of the spectrophotometer. From these results the two best operational parameters are the buffer/acid ratio of 10 and 15 and an acid concentration of 0.45 mol/L. The combination of $[H^+]$=0.45 mol/L and R=10 were selected and used for further experiments.

EFFECT OF GAS FLOW RATE, LIQUID FLOW RATE AND VISCOSITY ON THE MICROMIXING EFFICIENCY

The influence of three different operational parameters (i.e. gas flow rate, liquid flow rate and viscosity) on the micromixing efficiency is investigated with a fixed acid concentration (i.e. $[H^+]$=0.45 mol/L) and stream ratio (i.e. R=10). The gas flow rate (G) is varied from 30 to 90 Nm^3/hr, the buffer liquid flow rate (Q_{buffer}) from 4 to 10 kg/hr and the viscosity of the buffer stream from 1 to 3.7 mPa·s (using glycerin). A brief discussion on the pressure drop over the GLVR is provided in the supporting information to show the effect of gas flow and liquid flow on the overall pressure drop, which could be helpful for an understanding of the flow in the GLVR.

The influence of the first operating condition, the gas flow rate, is also displayed in **Figure 6b**. With increasing gas flow rates, the segregation index decreases indicating improved micromixing. To understand this phenomenon, one could understand the role of the gas phase in

the GLVR by comparing with a stirred tank and a rotating packed bed reactor. (1) In a stirred tank, the main energy input comes from the rotation of the impeller, creating a region with a high turbulent energy dissipation rate, which is beneficial to the micromixing efficiency [31,42]. In general, the liquid phase in the stirred tank is continuous. (2) In a rotating packed bed, the main energy input comes from the rotation of the rotor. For an air-water system, the liquid holdup is usually lower than 20% [43,44]. The high-speed rotation of the packing material (rotor) breaks the liquid into thin films, ligaments and droplets [45–47]. Therefore, the liquid phase in the rotating packed bed is discrete. It is worth mentioning that the role of the packing in rotating packed beds should be considered in conjunction with the design of liquid inlet distribution nozzles, as discussed in Wenzel et al.'s work [4,48]. Nevertheless, the micromixing process in a rotating packed bed is thus intensified as compared to a stirred tank [49]. (3) In the GLVR, the gas flow has a great influence on the mixing process due to the momentum transfer between the gas phase and the liquid phase. In other words, the gas flow is the main energy input for a GLVR and plays the role of the impeller or rotor in a stirred tank or rotating packed bed. The strong vortex gas flow breaks the liquid flow and disperses it in the GLVR chamber. The liquid phase is observed as the discrete phase during the experiments, which is closer to the liquid flow in a rotating packed bed. Increasing the gas flow rate increases the energy dissipation rate, resulting in a lower X_S and thus improves the micromixing efficiency. It is worth reminding that this dispersion condition is achieved in a static reactor geometry.

Figure 7a shows the effect of liquid flow rate on the micromixing efficiency in the GLVR. Both at the highest gas flow rate (i.e. 90 Nm^3/hr) and the lowest gas flow rate (i.e. 30 Nm^3/hr), the segregation index increases with increasing liquid flow rate, indicating a decrease in micromixing efficiency. After introducing the liquid flow, it needs to be accelerated by the gas to

a certain angular velocity. At a constant gas flow rate, increasing the liquid flowrate decreases the liquid angular velocity, resulting in lower slip velocities between gas and liquid, as a lower centrifugal force and less turbulence is induced. A lower shear force with the wall would also lead to less turbulence. Previous research in gas-solid vortex reactor [50] also shows that the gas flow changes from "multiple rotations" to "less than one full rotation" inside the unit chamber when increasing the solid loading from zero to the maximum capacity. This is referred to as the suppression of the primary gas flow of the jets and secondary flow of counterflow and backflow. Increasing the liquid flow rate is expected to exacerbate this effect. This decrease in turbulence can explain the decrease in micromixing efficiency with an increasing liquid flow rate as shown in **Figure 7a**.

Figure 7b shows the effect of the liquid viscosity on the micromixing efficiency in the GLVR. By increasing the glycerin mass fraction from 0 to 40 wt% (i.e. 1.0 to 3.7 mPa·s) the segregation index increases significantly. This effect, caused by a decrease of the deformation and shrinkage rate of liquid elements combined with a decrease of the molecular diffusion coefficients, has been established in previous studies [1,51,52]. From a macro scale perspective, a higher viscosity increases the viscous resistance and further aggravates the suppression effect of the gas flow. Numerical study [46] of a rotating packed bed showed that the effect of increasing the liquid viscosity on the liquid holdup is similar to the effect of increasing the liquid flow rate. Higher viscosities will increase the size of the liquid elements, resulting in poor micromixing conditions. This can also be expected in the GLVR.

MICROMIXING TIME ASSESSMENT

Using the incorporation model, the segregation indices (X_S) can be linked to a micromixing time (t_m). The relation between t_m and X_S is shown in **Figure 8** (solid line). **Figure 8** also shows all

the X_S values obtained under various operating conditions. The micromixing time of the GLVR ranges from 4.2×10^{-4} s to 3.3×10^{-3} s. For a gas flow rate of 90 Nm^3/s, a buffer liquid flow rate of 4 kg/h and a viscosity of 1.0 mPa·s, t_m reaches a minimum value. The micromixing time should be compared with the reaction characteristic time of the Villermaux-Dushman reaction system to justify the chosen acid concentration and buffer to acid stream ratio, which is provided in the supporting information.

As discussed by Bourne in 2008 [37], the micromixing time can be used to rank different mixers and reactors based on their micromixing performance. However, the influence of the micromixing model (such as the incorporation model used in this work), the inserted kinetic parameters, and the operating conditions is not negligible. Therefore, a comparison based on the order of magnitude rather than the absolute values is necessary. In such a comparison, the micromixing time of the GLVR is presented as 10^{-4}~10^{-3} s. The order of magnitudes of the micromixing time for various reactors and mixers is shown in **Table 4**. From this comparison, it follows that the GLVR has the potential to be used in micromixing controlled applications.

Note that the mean residence time in the premix pipe is approximately 0.1 s, which is higher than the calculated micromixing time or the reaction characteristic time. However, the Reynolds number of the premixed stream is 883, even at the highest liquid flow rate and the lowest liquid viscosity, implying that the flow in the premix tube is laminar under all the studied operating conditions. The conversion in the premix tube is thus rather limited due to the laminar flow condition as the two liquid streams are converging rather than mixing [55], the main mixing-reaction process therefore occurs in the GLVR chamber. Meanwhile, it should be noted that the premixing of the two streams is necessary to ensure that the two streams contact and mix in the

reactor chamber. Similar design suggestions could be found in previous micromixing studies of rotating packed beds [56–58].

Estimating the energy dissipation rate of the GLVR can further assess the efficiency of the vortex unit used as a mixer, which can be calculated as [5,59,60]:

$$\varepsilon = \frac{P_{input}}{\rho V_L} \tag{10}$$

where ε (W/kg) is the energy dissipation rate per mass unit of the liquid phase, P_{input} (W) is the power input, ρ is the density of the liquid phase and V_L is the liquid holdup volume in the GLVR. The P_{input} is given by:

$$P_{input} = G\Delta P + \frac{1}{2}L(v_{in}^2 - v_{out}^2) \tag{11}$$

In Eq. 11 the first term on the right-hand side is the main energy input to the GLVR from the gas phase. The second term is the momentum change of the liquid phase, which is much lower than the first term and is negligible. G is the volumetric gas flow rate (m^3/s), ΔP is the measured pressure drop, L is the mass liquid flow rate (kg/s), v_{in}^2 is the liquid inlet velocity and v_{out}^2 is the liquid outlet velocity.

Obtaining the liquid holdup volume in a reactor or mixer often requires non-intrusive techniques or residence time measurement [43,61]. Nevertheless, the liquid holdup volume in the GLVR can be approximated via assessment of the conservation of kinetic energy between the gas and liquid phase. Due to the high gas-liquid ratio in this work, a low liquid holdup is observed during experiments. Therefore, the following assumptions are proposed: (1) The loss of gas energy is converted into increased kinetic energy of the liquid; (2) The liquid is accelerated by the gas and the liquid outlet velocity is the same as the gas outlet velocity; (3) The mean residence time of

the gas phase is calculated based on the whole GLVR chamber volume *V*. As such, the V_L can be estimated as:

$$V_L = \frac{G\Delta P * \tau_g}{\frac{1}{2}\rho\left(v_{out}^2 - v_{in}^2\right)} \quad (12)$$

where the mean residence time of the gas phase is given by:

$$\tau_g = \frac{V}{G} \quad (13)$$

and liquid inlet and outlet velocity are given by:

$$v_{in} = \frac{L}{\frac{1}{4}\rho\pi D_L^2} \quad (14)$$

$$v_{out} = \frac{G}{\frac{1}{4}\pi D_E^2} \quad (15)$$

To make sure the above assumptions are reasonable, the measured pressure drop values are used to calculate liquid holdup volume. Calculations from Eqs. 12-15 indicate the liquid holdup (V_L/V) in the GLVR ranges from 9% to 21% under various operating conditions. The liquid holdup values qualitatively agree with observations from the viewing window and the values reported in other similar reactors or mixers [43,62], indicating the above assumptions can be accepted for a rough estimation.

Figure 9 shows the micromixing time versus the energy dissipation rate estimated from the above equations. In Falk and Commenge's work [5], a correlation between the micromixing time and the dissipation rate was proposed, shown as the solid line in **Figure 9.** It has been found the data points in various reactors or mixers are within ±30% near this solid line, meaning the price of a lower micromixing time is often with a higher energy dissipation rate. More importantly, the area to the left of the solid line indicates a higher energetic efficiency, suggesting the energetic

efficiency of the GLVR could be advantageous. Nevertheless, based on Eq. 10 and the three assumptions, the estimated energy dissipation rate in could be lower than the actual values due to energy losses not taken into account and over-estimated liquid outlet velocity. As a result, the data points in this work in **Figure 9** may need to be shifted to the right by a certain margin.

CONCLUSIONS AND OUTLOOK

The micromixing performance for multiphase process of the GLVR is assessed and confirmed by the Villermaux-Dushman protocol. After establishing a proper combination of acid concentration and acid to buffer stream ratio, the effect of gas flow rate, liquid flow rate and the buffer stream viscosity on the segregation index has been optimized. The results indicate that high driver gas flow rates, low liquid flow rates and a low liquid viscosity favor micromixing. The experimental results are coupled with the incorporation model to estimate the micromixing time of the GLVR. Using this model, the order of magnitude of the GLVR's micromixing time is in the order of 10^{-4}~10^{-3} s. This order of magnitude coincided with the order of other advanced reactors such as the ultrasound aided reactor or the rotating packed bed. The estimation of the energy dissipation rate indicates the energetic efficiency of the GLVR could be advantageous when using the GLVR as a mixer, but this should be further confirmed after obtaining an accurate measurement of the liquid holdup. Results in this work provide a fundamental guideline of using the vortex units for possible liquid micromixing applications.

In future work the performance of the GLVR will be further improved by addressing detailed flow information and optimizing the reactor geometry, including studies on hydrodynamics of the gas-liquid flow, analyzing the residence time distribution of the liquid stream and optimization of the liquid premixing.

LIST OF FIGURE CAPTIONS

LIST OF TABLE CAPTIONS

NOMENCLATURE

X_S	segregation index
R	volumetric flow ratio of the buffer stream and the Acid stream
R1	neutralization reaction of the iodide-iodate reaction system
R2	redox-reaction of the iodide-iodate reaction system
R3	equilibrium reaction of the iodide-iodate reaction system
Q_{buffer}	mass flow rate of the buffer stream, kg/h
G	gas flow rate, Nm^3/h or Nm^3/s
L	total liquid flow rate, kg/h or kg/s
t_m	micromixing characteristic time, s
t_{R1}	reaction characteristic time of R1, s
t_{R2}	reaction characteristic times of R2, s
g	growth rate of the reactional volume in the incorporation model
C_j	concentration of species *j*, $kmol/m^3$
R_j	net production rate of species *j*, $kmol/(m^3 \cdot s)$

ACKNOWLEDGMENTS

The research leading to these results has received funding from the European Research Council under the European Union's Horizon 2020 research and innovation programme / ERC grant agreement n° 818607.

REFERENCES

1. Wenzel D, Górak A. Review and analysis of micromixing in rotating packed beds. *Chem*

Eng J. 2018;345(March):492-506. doi:10.1016/j.cej.2018.03.109

2. Mao Z, Yang C. Micro-mixing in chemical reactors: A perspective. *Chinese J Chem Eng*. 2017;25(4):381-390. doi:10.1016/j.cjche.2016.09.012
3. Johnson BK, Prud'homme RK. Chemical processing and micromixing in confined impinging jets. *AIChE J*. 2003;49(9):2264-2282. doi:10.1002/aic.690490905
4. Wenzel D, Nolte K, Górak A. Reactive mixing in rotating packed beds: On the packing's role and mixing modeling. *Chem Eng Process - Process Intensif*. 2019;143(July):107596. doi:10.1016/j.cep.2019.107596
5. Falk L, Commenge JM. Performance comparison of micromixers. *Chem Eng Sci*. 2010;65(1):405-411. doi:10.1016/j.ces.2009.05.045
6. Liu Y, Luo Y, Chu G, Luo J, Arowo M, Chen J. 3D numerical simulation of a rotating packed bed with structured stainless steel wire mesh packing. *Chem Eng Sci*. 2017;170:365-377. doi:10.1016/j.ces.2017.01.033
7. Stankiewicz AI, Moulijn JA. Process intensification: transforming chemical engineering. *Chem Eng Prog*. 2000;96(1):22-34.
8. Gonzalez-Quiroga A, Reyniers PA, Kulkarni SR, et al. Design and cold flow testing of a Gas-Solid Vortex Reactor demonstration unit for biomass fast pyrolysis. *Chem Eng J*. 2017;329:198-210. doi:10.1016/j.cej.2017.06.003
9. Ashcraft RW, Heynderickx GJ, Marin GB. Modeling fast biomass pyrolysis in a gas-solid vortex reactor. *Chem Eng J*. 2012;207-208:195-208. doi:10.1016/j.cej.2012.06.048
10. Kulkarni SR, Vandewalle LA, Gonzalez-quiroga A, et al. Computational Fluid Dynamics-Assisted Process Intensification Study for Biomass Fast Pyrolysis in a Gas−Solid Vortex Reactor. *Energy & Fuels*. 2018;32:10169-10183. doi:10.1021/acs.energyfuels.8b01008

11. Dutta A, Ekatpure RP, Heynderickx GJ, de Broqueville A, Marin GB. Rotating fluidized bed with a static geometry: Guidelines for design and operating conditions. *Chem Eng Sci*. 2010;65(5):1678-1693. doi:10.1016/j.ces.2009.11.013

12. Ekatpure RP, Suryawanshi VU, Heynderickx GJ, de Broqueville A, Marin GB. Experimental investigation of a gas-solid rotating bed reactor with static geometry. *Chem Eng Process Process Intensif*. 2011;50(1):77-84. doi:10.1016/j.cep.2010.11.010

13. Ashcraft RW, Kovacevic J, Heynderickx GJ, Marin GB. Assessment of a gas-solid vortex reactor for SO2/NOx adsorption from flue gas. *Ind Eng Chem Res*. 2013;52(2):861-875. doi:10.1021/ie300399w

14. Kovacevic JZ, Pantzali MN, Niyogi K, Deen NG, Heynderickx GJ, Marin GB. Solids velocity fields in a cold-flow gas-solid vortex reactor. *Chem Eng Sci*. 2015;123:220-230. doi:10.1016/j.ces.2014.10.020

15. Pantzali MN, Kovacevic JZ, Heynderickx GJ, Marin GB, Shtern VN. Radial pressure profiles in a cold-flow gas-solid vortex reactor. *AIChE J*. 2015;61(12):4114-4125. doi:10.1002/aic.14912

16. Niyogi K, Torregrosa MM, Pantzali MN, Heynderickx GJ, Marin GB. Experimentally validated numerical study of gas-solid vortex unit hydrodynamics. *Powder Technol*. 2017;305(x):794-808. doi:10.1016/j.powtec.2016.10.049

17. Friedle M, Marin GB, Heynderickx GJ. Operational range of a Gas-Solid Vortex Unit. *Powder Technol*. 2018;338:702-715. doi:10.1016/j.powtec.2018.07.062

18. Friedle M, Niyogi K, Torregrosa MM, Marin GB, Heynderickx GJ. A drag model for the gas-solid vortex unit. *Powder Technol*. 2017;312:210-221. doi:10.1016/j.powtec.2017.02.012

19. Kuzmin AO, Pravdina MK, Yavorsky AI, Yavorsky NI, Parmon VN. Vortex centrifugal bubbling reactor. *Chem Eng J*. 2005;107(1-3):55-62. doi:10.1016/j.cej.2004.12.010

20. Vangaever S. Numerical Parametric Study of Fast Biomass Pyrolysis in a Gas Solid Vortex Reactor. Published online 2016.

21. Fang JZ, Lee DJ. Micromixing efficiency in static mixer. *Chem Eng Sci*. 2001;56(12):3797-3802. doi:10.1016/S0009-2509(01)00098-7

22. Yang M, Luo L, Chen G. Microfluidic synthesis of ultrasmall Co nanoparticles over reduced graphene oxide and their catalytic properties. *AIChE J*. 2020;66(6). doi:10.1002/aic.16950

23. Bovone G, Guzzi EA, Tibbitt MW. Flow-based reactor design for the continuous production of polymeric nanoparticles. *AIChE J*. 2019;65(12):1-13. doi:10.1002/aic.16840

24. Yin X, Sun Q, Wang D, et al. High-gravity-assisted synthesis of aqueous nanodispersions of organic fluorescent dyes for counterfeit labeling. *AIChE J*. 2019;65(10):14-16. doi:10.1002/aic.16714

25. Chen H, Diep E, Langrish TAG, Glasser BJ. Continuous fluidized bed drying: Residence time distribution characterization and effluent moisture content prediction. *AIChE J*. 2020;66(5). doi:10.1002/aic.16902

26. Jeong GS, Chung S, Kim CB, Lee SH. Applications of micromixing technology. *Analyst*. 2010;135(3):460-473. doi:10.1039/b921430e

27. Tuo L, Ruan X, Xiao W, Li X, He G, Jiang X. A novel hollow fiber membrane-assisted antisolvent crystallization for enhanced mass transfer process control. *AIChE J*. 2019;65(2):734-744. doi:10.1002/aic.16438

28. Fournier MC, Falk L, Villermaux J. A new parallel competing reaction system for

assessing micromixing efficiency-determination of micromixing time by a simple mixing model. *Chem Eng Sci*. 1996;51(23):5187-5192. doi:10.1016/S0009-2509(96)00340-5

29. Bourne JR, Kozicki F, Rys P, et al. Mixing and fast chemical reaction-I test reactions to determine segregation. *Chem Eng Sci*. 1981;36(Id):1643-1648. doi:10.1016/0009-2509(81)80008-5

30. Zhang H, Kopfmüller T, Achermann R, et al. Accessing multidimensional mixing via 3D printing and showerhead micromixer design. *AIChE J*. 2020;66(4). doi:10.1002/aic.16873

31. Bourne JR, Yu S. Investigation of micromixing in stirred tank reactors using parallel reactions. *Ind Eng Chem Res*. 1994;33(1):41-55. doi:10.1021/ie00025a007

32. Guichardon P, Falk L, Villermaux J. Characterisation of micromixing efficiency by the iodide–iodate reaction system. Part II: kinetic study. *Chem Eng Sci*. 2000;55(19):4245-4253. doi:10.1016/S0009-2509(00)00069-5

33. Guichardon P, Falk L. Characterisation of micromixing efficiency by the iodide - iodate reaction system . Part I: experimental procedure. *Chem Eng Sci*. 2000;55(19):4233-4243. doi:10.1016/S0009-2509(00)00068-3

34. Palmer DA, Ramette RW, Mesmer RE. Triiodide ion formation equilibrium and activity coefficients in aqueous solution. *J Solution Chem*. 1984;13(9):673-683. doi:10.1007/BF00650374

35. Kölbl A, Desplantes V, Grundemann L, Scholl S. Kinetic investigation of the Dushman reaction at concentrations relevant to mixing studies in stirred tank reactors. *Chem Eng Sci*. 2013;93:47-54. doi:10.1016/j.ces.2013.01.067

36. Kölbl A, Kraut M, Dittmeyer R. Kinetic investigation of the Dushman reaction at concentrations relevant to mixing studies in microstructured cyclone type mixers. *Chem*

Eng Sci. 2013;101:454-460. doi:10.1016/j.ces.2013.07.008

37. Bourne JR. Comments on the iodide/iodate method for characterising micromixing. *Chem Eng J*. 2008;140(1-3):638-641. doi:10.1016/j.cej.2008.01.031

38. Kölbl A, Schmidt-Lehr S. The iodide iodate reaction method: The choice of the acid. *Chem Eng Sci*. 2010;65(5):1897-1901. doi:10.1016/j.ces.2009.11.032

39. Wenzel D, Assirelli M, Rossen H, Lopattschenko M, Górak A. On the reactant concentration and the reaction kinetics in the Villermaux-Dushman protocol. *Chem Eng Process - Process Intensif*. 2018;130:332-341. doi:10.1016/j.cep.2018.06.022

40. Pinot J, Commenge JM, Portha JF, Falk L. New protocol of the Villermaux-Dushman reaction system to characterize micromixing effect in viscous media. *Chem Eng Sci*. 2014;118:94-101. doi:10.1016/j.ces.2014.07.010

41. Baqueiro C, Ibaseta N, Guichardon P, Falk L. Influence of reagents choice (buffer, acid and inert salt) on triiodide production in the Villermaux-Dushman method applied to a stirred vessel. *Chem Eng Res Des*. 2018;136(2000):25-31. doi:10.1016/j.cherd.2018.04.017

42. Han Y, Wang JJ, Gu XP, Feng LF. Numerical simulation on micromixing of viscous fluids in a stirred-tank reactor. *Chem Eng Sci*. 2012;74:9-17. doi:10.1016/j.ces.2012.02.018

43. Yang Y, Xiang Y, Chu G, Zou H, Luo Y. A noninvasive X-ray technique for determination of liquid holdup in a rotating packed bed. *Chem Eng Sci*. 2015;138:244-255. doi:10.1016/j.ces.2015.07.044

44. Burns JR, Jamil JN, Ramshaw C. Process intensification: Operating characteristics of rotating packed beds - determination of liquid hold-up for a high-voidage structured

packing. *Chem Eng Sci*. 2000;55(13):2401-2415. doi:10.1016/S0009-2509(99)00520-5

45. Burns JR, Ramshaw C. Process intensification: visual study of liquid maldistribution in rotating packed beds. *Chem Eng Sci*. 1996;51(8):1347-1352. doi:10.1016/0009-2509(95)00367-3

46. Ouyang Y, Zou H-K, Gao X-Y, Chu G-W, Xiang Y, Chen J-F. Computational fluid dynamics modeling of viscous liquid flow characteristics and end effect in rotating packed bed. *Chem Eng Process Process Intensif*. 2017;123:185-194. doi:10.1016/j.cep.2017.09.005

47. Xie P, Pourkashanian M, Yang X, et al. A mesoscale 3D CFD analysis of the liquid flow in a rotating packed bed. *Chem Eng Sci*. 2019;199:528-545. doi:10.1016/j.ces.2019.01.038

48. Wenzel D, Gerdes N, Steinbrink M, Ojeda LS, Górak A. Liquid Distribution and Mixing in Rotating Packed Beds. *Ind Eng Chem Res*. 2019;58(15):5919-5928. doi:10.1021/acs.iecr.8b04025

49. Zhao H, Shao L, Chen J-FF. High-gravity process intensification technology and application. *Chem Eng J*. 2010;156(3):588-593. doi:10.1016/j.cej.2009.04.053

50. Kulkarni SR, Gonzalez-Quiroga A, Nuñez M, et al. An experimental and numerical study of the suppression of jets, counterflow, and backflow in vortex units. *AIChE J*. 2019;65(8):1-13. doi:10.1002/aic.16614

51. Monnier H, Wilhelm AM, Delmas H. Effects of ultrasound on micromixing in flow cell. *Chem Eng Sci*. 2000;55(19):4009-4020. doi:10.1016/S0009-2509(00)00067-1

52. Baldyga J, Bourne JR. Simplification of micromixing calculations. I. Derivation and application of new model. *Chem Eng J*. 1989;42(2):83-92. doi:10.1016/0300-9467(89)85002-6

53. Krupa K, Nunes MI, Santos RJ, Bourne JR. Characterization of micromixing in T-jet mixers. *Chem Eng Sci*. 2014;111:48-55. doi:10.1016/j.ces.2014.02.018

54. Chu GW, Song YJ, Zhang WJ, et al. Micromixing Efficiency Enhancement in a Rotating Packed Bed Reactor with Surface-Modified Nickel Foam Packing. *Ind Eng Chem Res*. 2015;54(5):6-11. doi:10.1021/ie504407a

55. Ouyang Y, Xiang Y, Gao XY, et al. Micromixing efficiency optimization of the premixer of a rotating packed bed by CFD. *Chem Eng Process - Process Intensif*. 2019;142(15):107543. doi:10.1016/j.cep.2019.107543

56. Jiao W, Liu Y, Qi G. Micromixing efficiency of viscous media in novel impinging stream-rotating packed bed reactor. *Ind Eng Chem Res*. 2012;51(20):7113-7118. doi:10.1021/ie202586f

57. Jiao W, Liu Y, Qi G. A new impinging stream–rotating packed bed reactor for improvement of micromixing iodide and iodate. *Chem Eng J*. 2010;157(1):168-173.

58. Yang K, Chu GW, Shao L, Luo Y, Chen JF. Micromixing efficiency of rotating packed bed with premixed liquid distributor. *Chem Eng J*. 2009;153(1-3):222-226. doi:10.1016/j.cej.2009.06.006

59. Commenge J-MM, Falk L. Villermaux–Dushman protocol for experimental characterization of micromixers. *Chem Eng Process Process Intensif*. 2011;50(10):979-990. doi:10.1016/j.cep.2011.06.006

60. Nie A, Gao Z, Xue L, Cai Z, Evans GM, Eaglesham A. Micromixing performance and the modeling of a confined impinging jet reactor/high speed disperser. *Chem Eng Sci*. 2018;184:14-24. doi:10.1016/j.ces.2018.03.032

61. Singh BK, Jain E, Buwa V V. Feasibility of Electrical Resistance Tomography for

measurements of liquid holdup distribution in a trickle bed reactor. *Chem Eng J*. 2019;358:564-579. doi:10.1016/j.cej.2018.10.009

62. Kuzmin AO. Confined multiphase swirled flows in chemical engineering. *Rev Chem Eng*. Published online 2020. doi:10.1515/revce-2019-0019

Table 1 *Reaction kinetics of the Villermaux-Dushman protocol* [32]

Rate equation	Kinetic parameters
$r_1 = k_1[\mathrm{H^+}][\mathrm{H_2BO_3^-}]$	$k_1 = 10^{11}\ m^3/kmol \cdot s$
$r_2 = k_2[\mathrm{IO_3^-}][\mathrm{H^+}]^2[\mathrm{I^-}]^2$	$\log k_2 = 9.281 - 3.664\sqrt{I}; I \leq 0.166$ M $\log k_2 = 8.383 - 1.511\sqrt{I} + 0.237I; I \geq 0.166$ M
$r_3 = k_3[\mathrm{I^-}][\mathrm{I_2}] - k_4[\mathrm{I_3^-}]$	$k_3 = 5.9 \times 10^9\ m^3/kmol \cdot s$ $k_4 = 7.5 \times 10^6\ s^{-1}$

Table 2 *Geometrical parameters and operating ranges of the GLVR*

Parameter	Value
Reactor diameter D_R (mm)	139
Reactor length H (mm)	25
Liquid inlet diameter D_L (mm)	4
Premix length L (mm)	20
Exhaust diameter D_E (mm)	40
Number of gas inlet slot	16
Slot width (mm)	1
Slot angle (°)	2.5
Gas flow rate (Nm^3/h)	30-90
Total liquid mass flow rate (kg/h)	4-12

Table 3 *Concentration of the acid and buffer solution*

	Components	Concentration
Components for buffer solution preparation	KIO_3 (mol/L)	0.00233
	KI (mol/L)	0.0117
	H_3BO_3 (mol/L)	0.1818
	NaOH (mol/L)	0.0909
	Glycerine (wt %)	0, 20, 30, 40
Component for acid solution preparation	$HClO_4$ (mol/L)	0.25, 0.35, 0.45

Table 4 *Comparison of the micromixing time of various reactors and mixers*

Reactors or mixers	Order of magnitude of the micromixing time [s]	Reference
Stirred vessel	10^{-2}	Guichardon et al. [32]
T-jet mixers	10^{-2}	Krupa et al. [53]
Kenics static mixer	10^{-3}	Fang et al. [21]
Ultrasound aided reactor	10^{-3}	Monnier et al. [51]
Rotating packed bed	10^{-4}~10^{-3}	Yang et al. and Chu et al. [43,54]
GLVR	10^{-4}~10^{-3}	This work

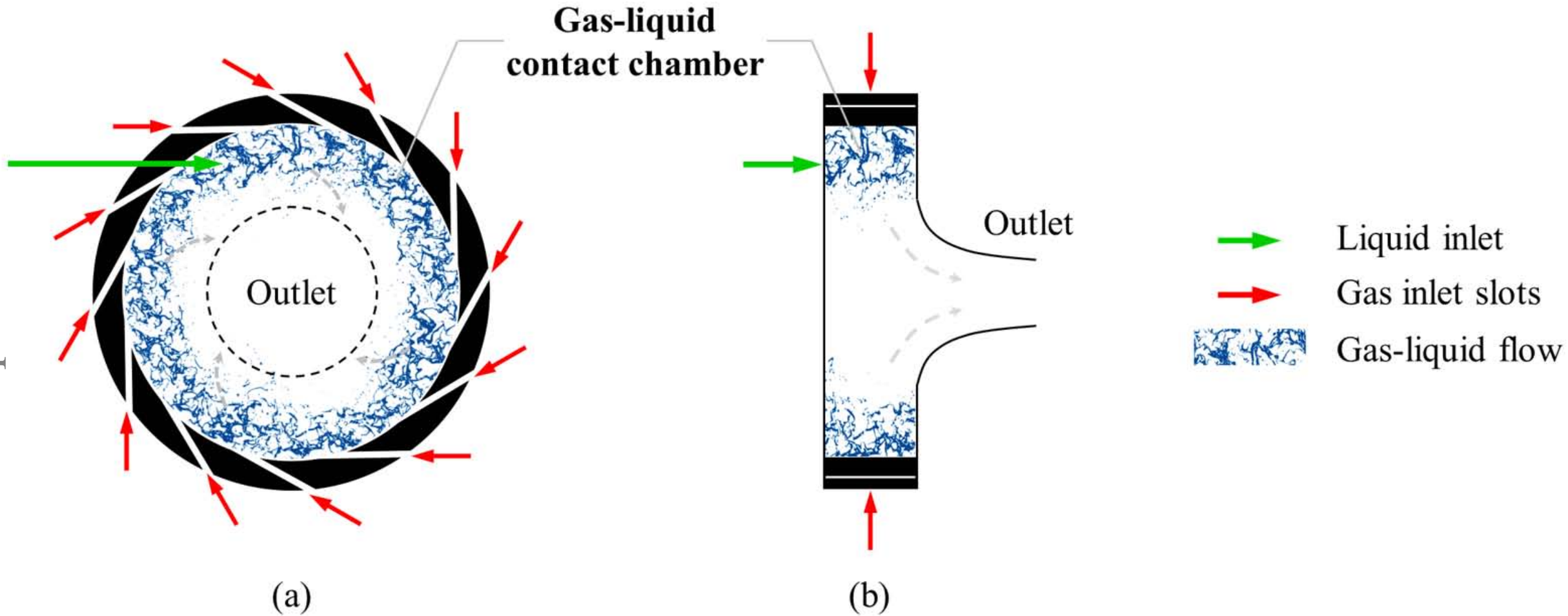

Villermaux-Dushman reaction system

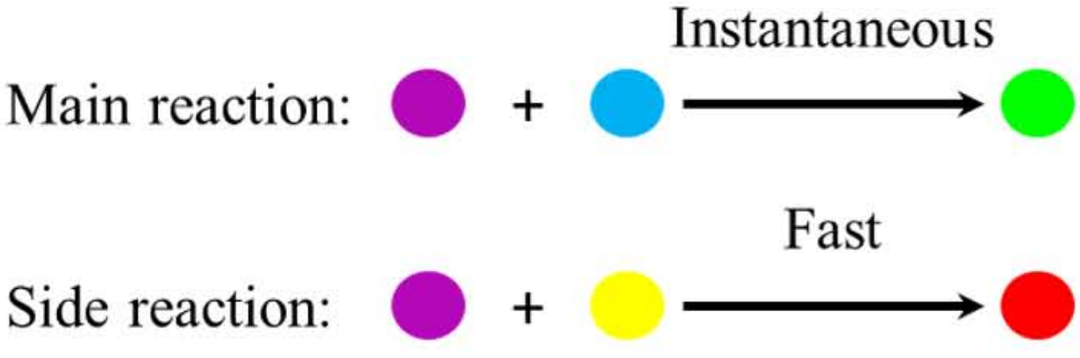

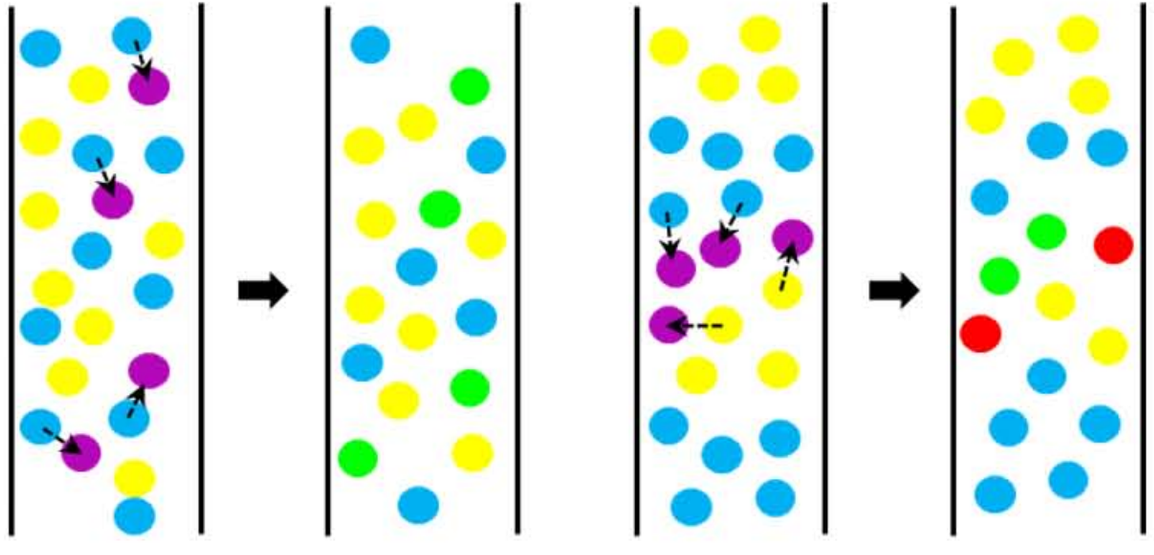

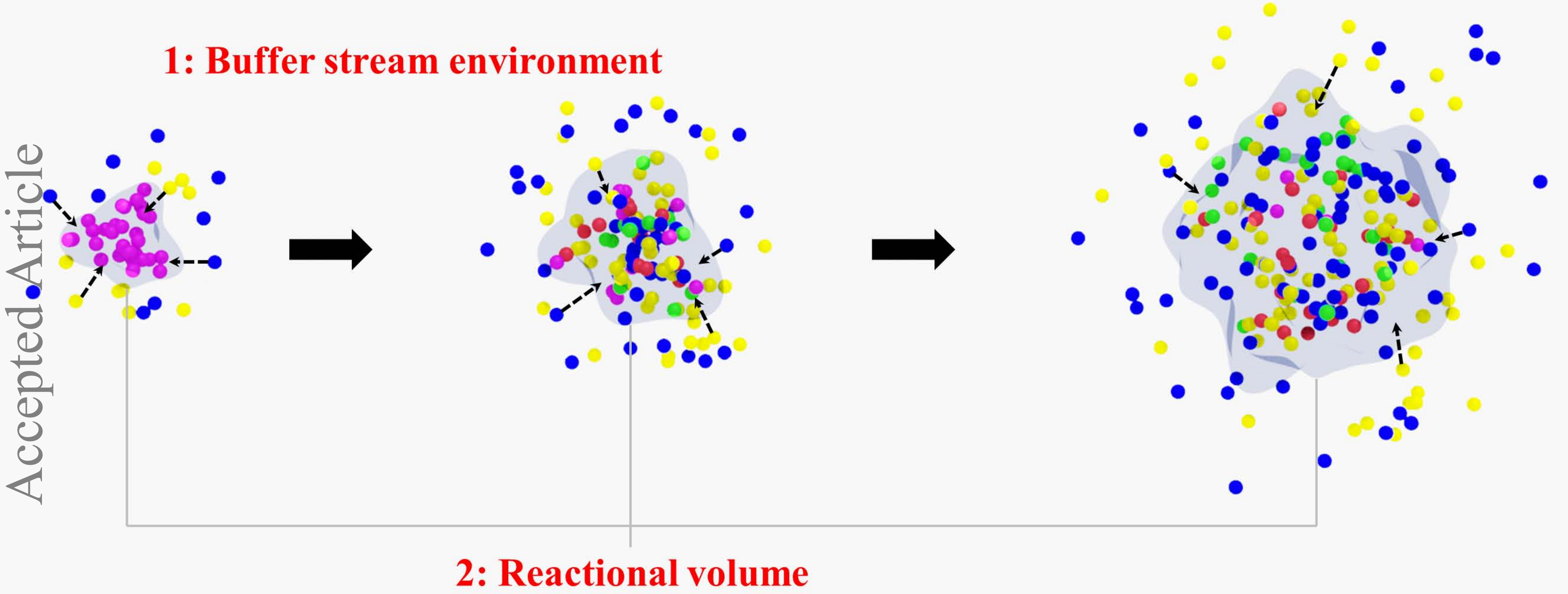

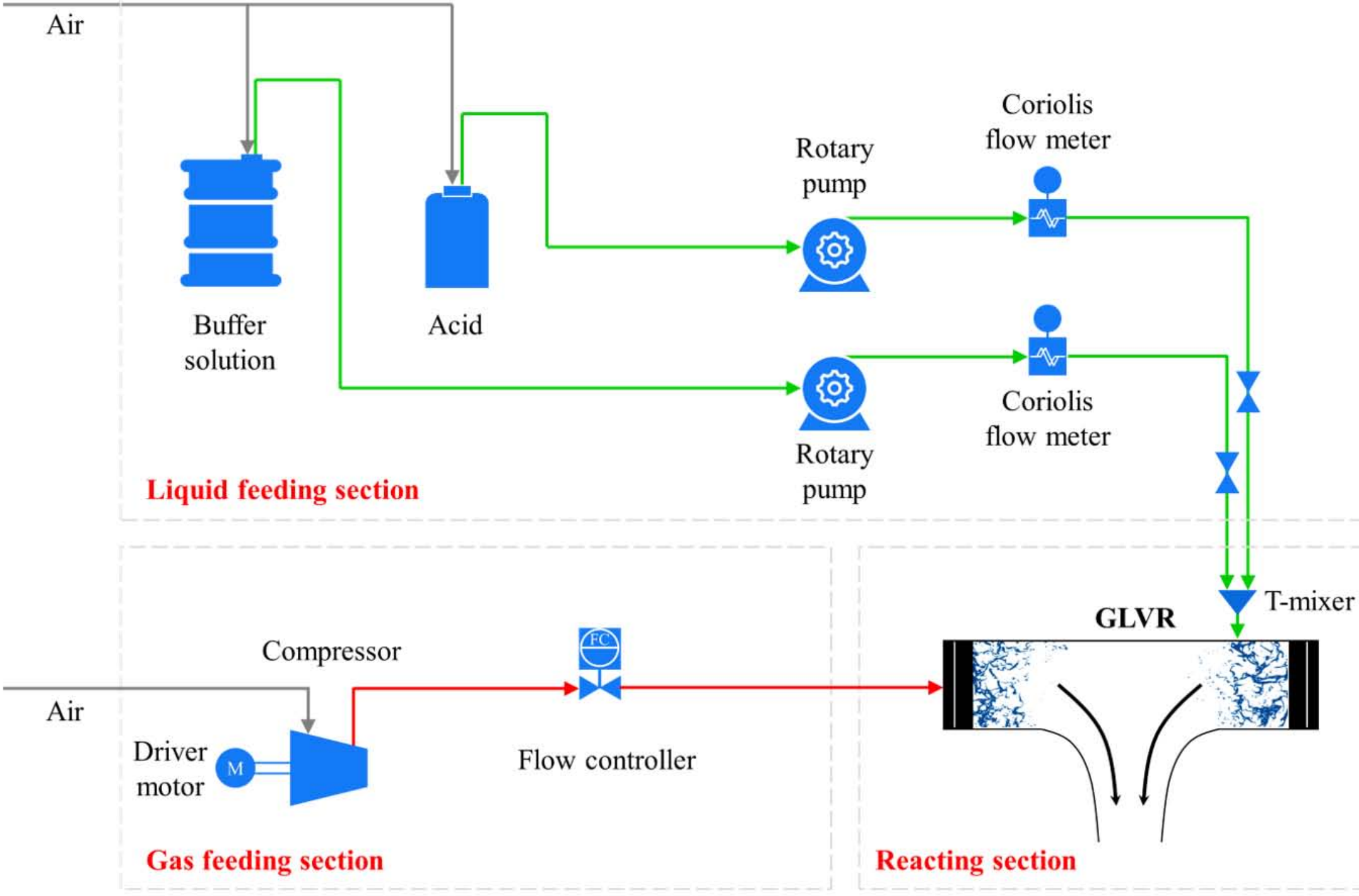

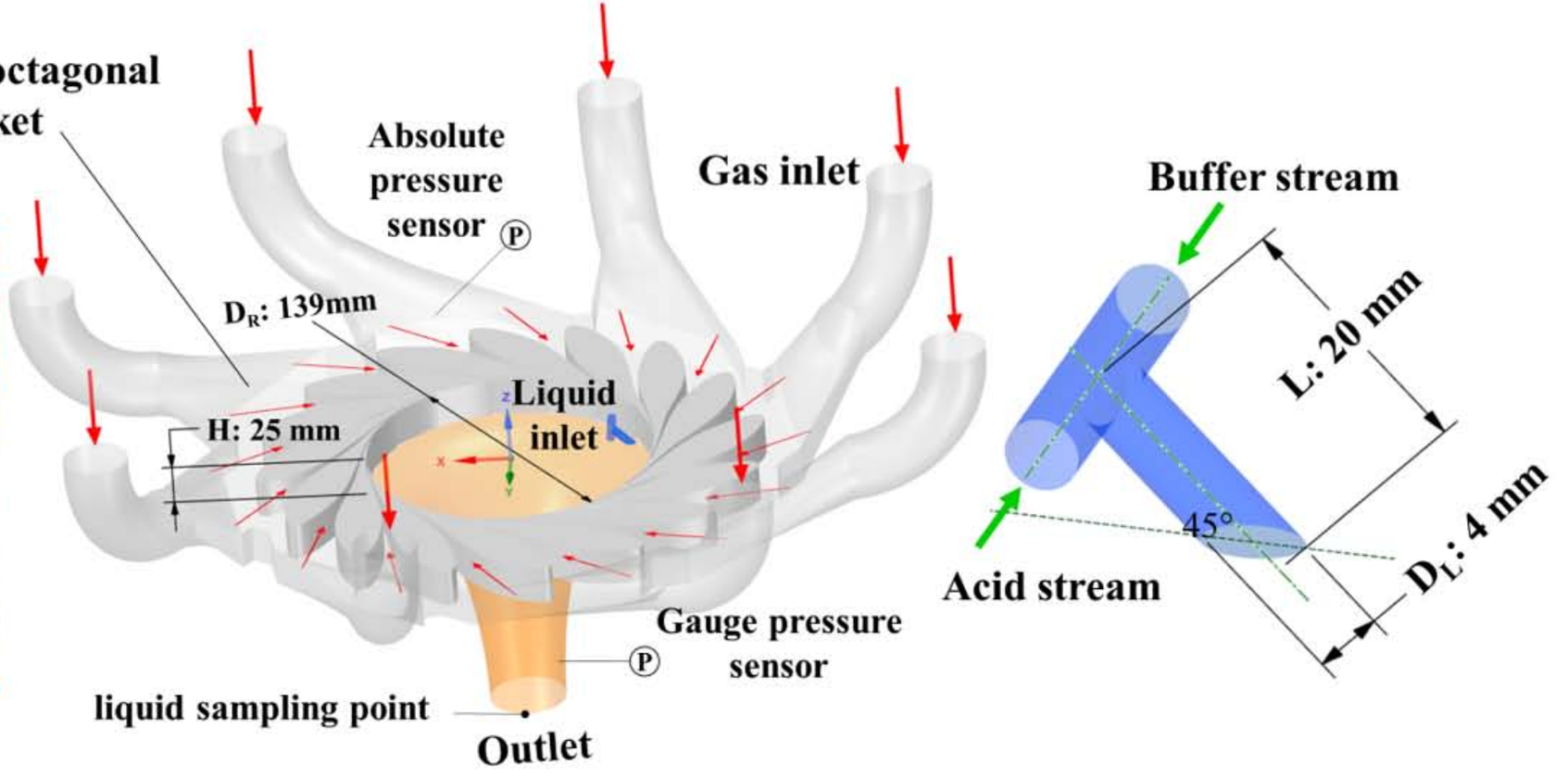

(a) (b) (c)

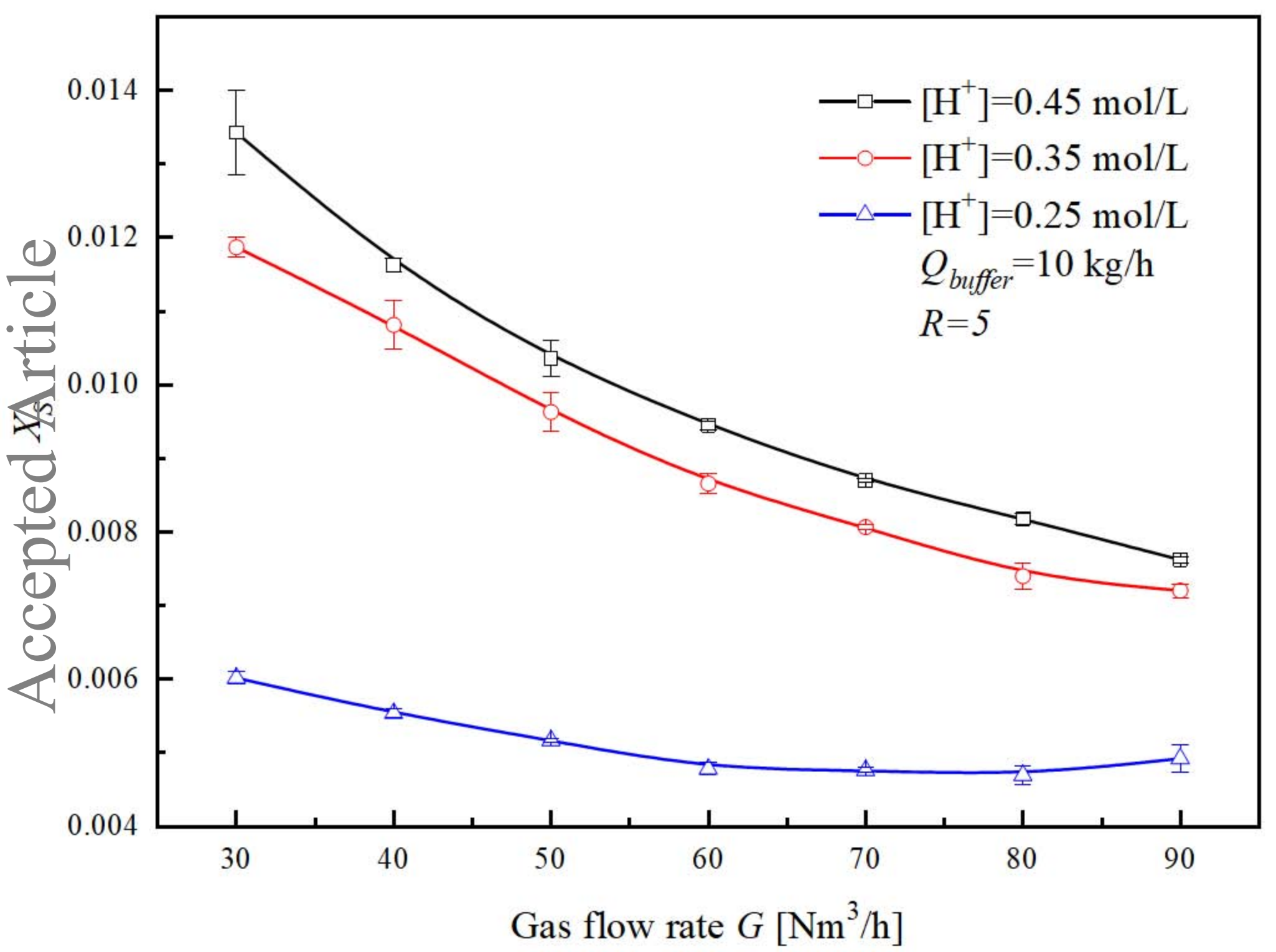

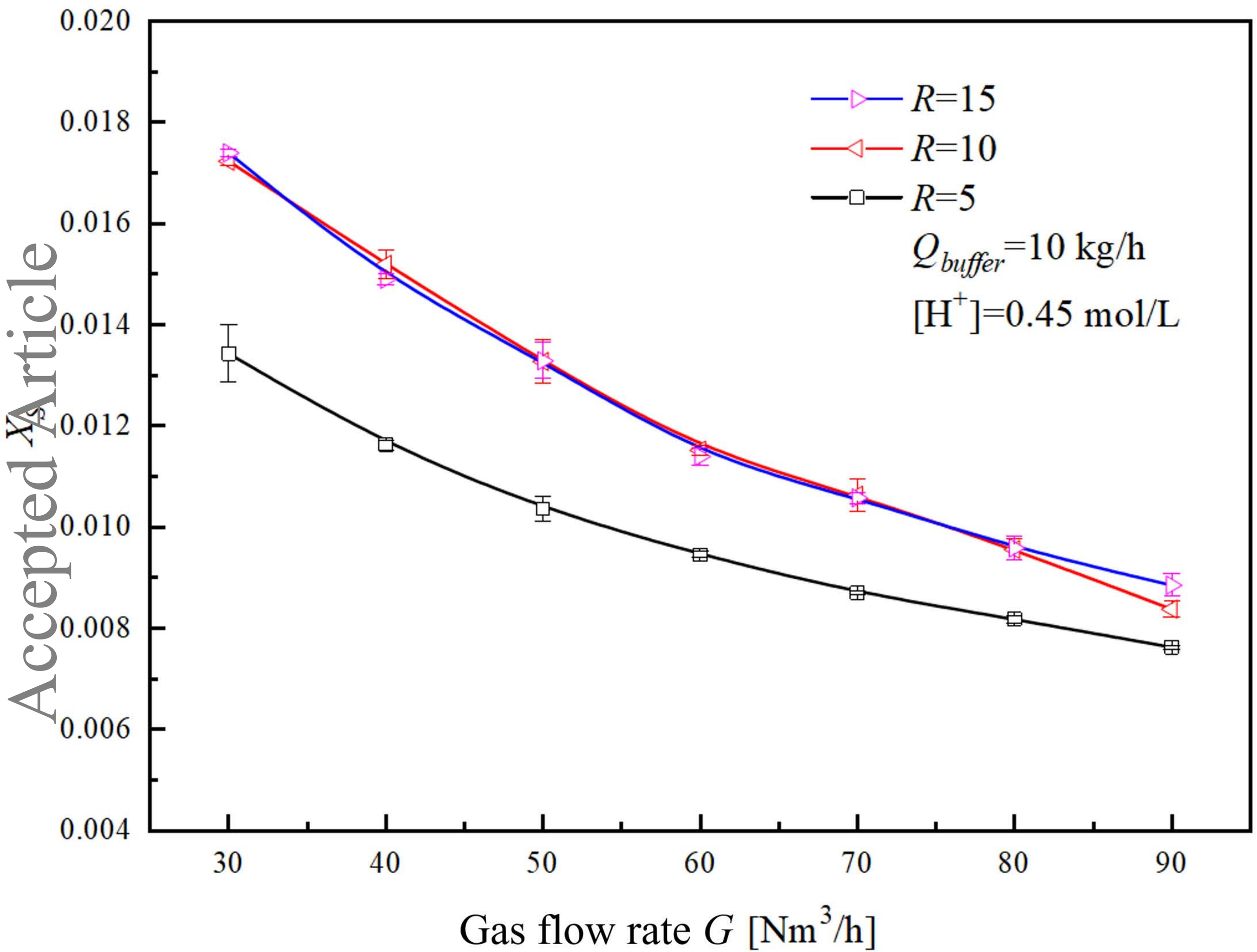

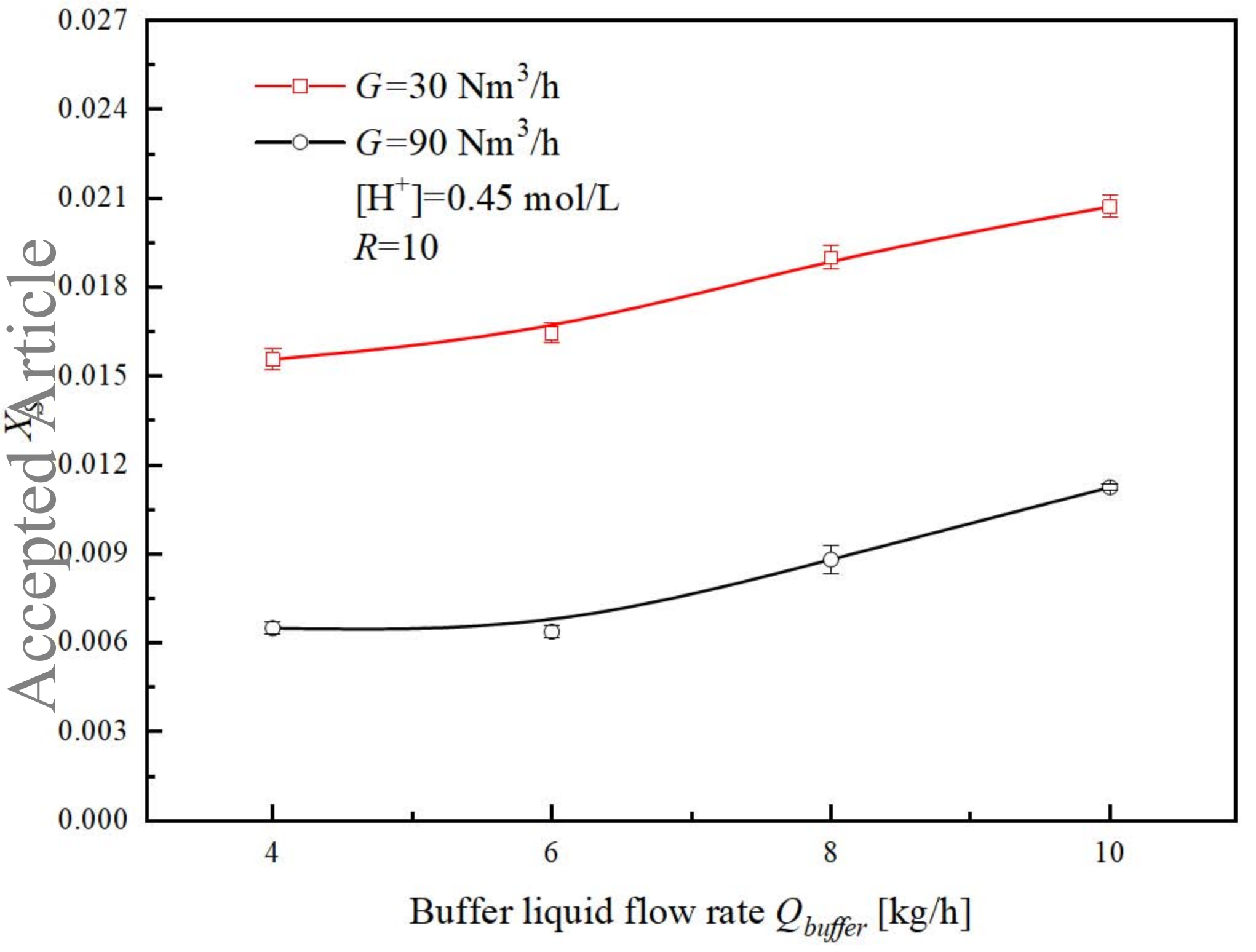

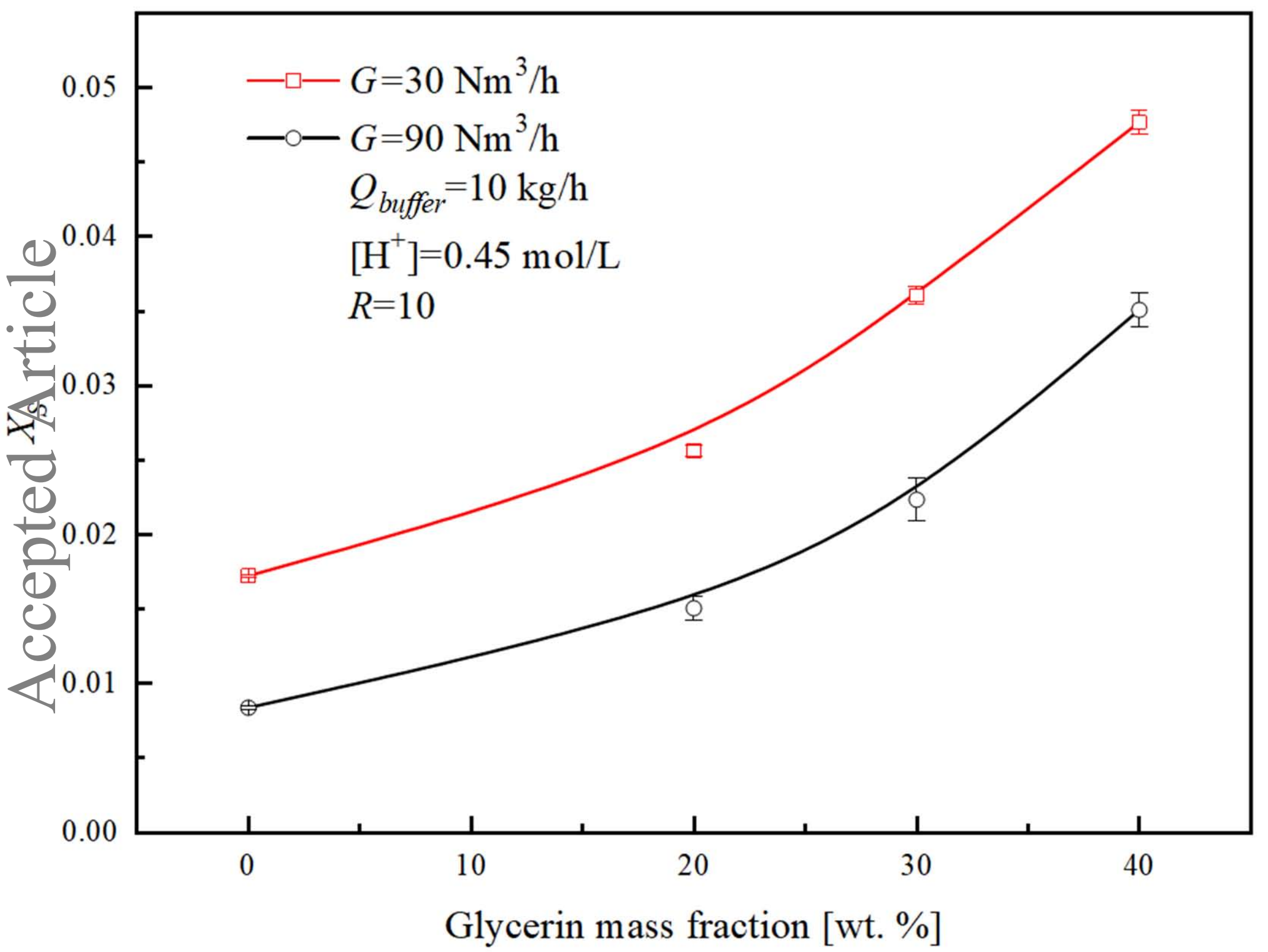

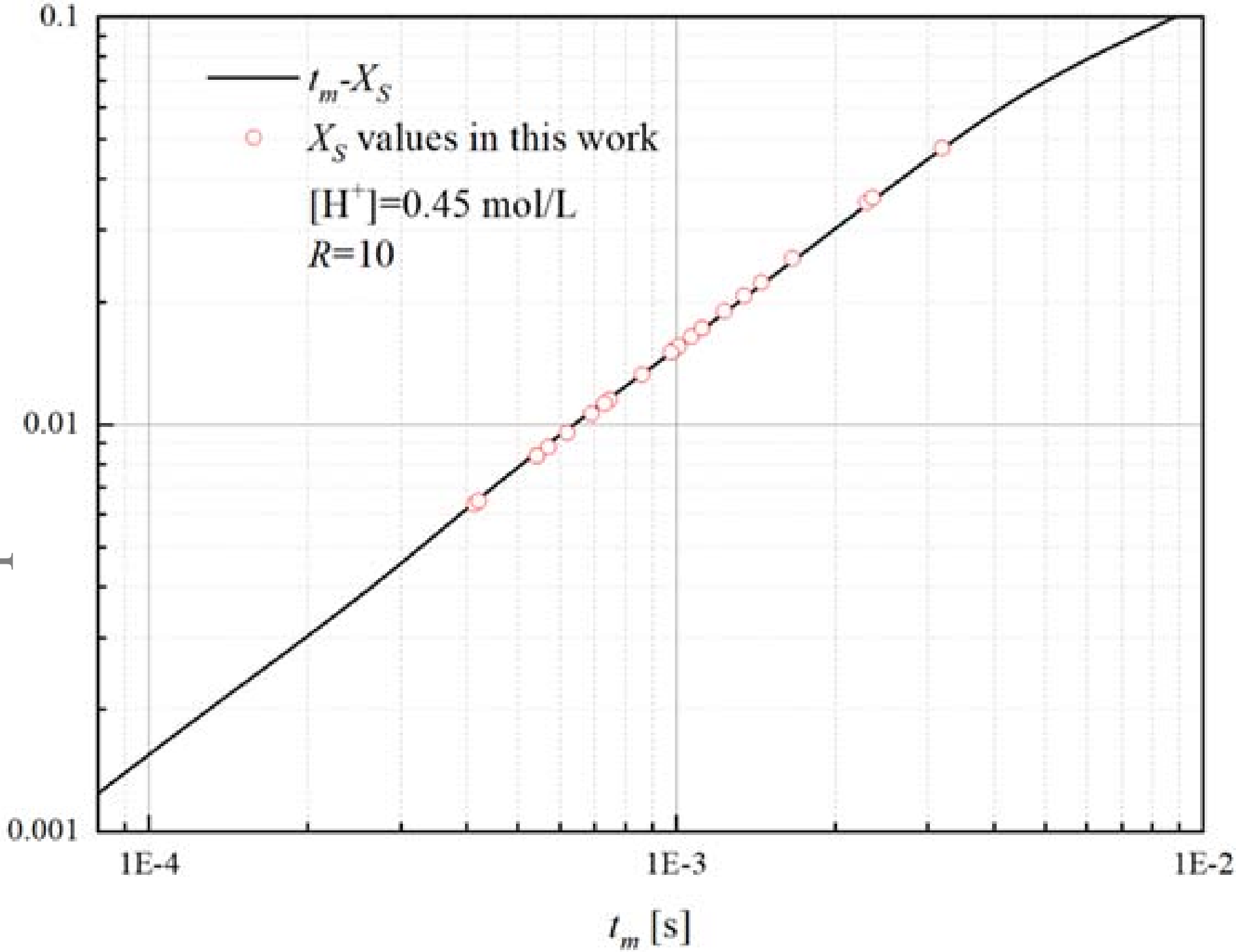

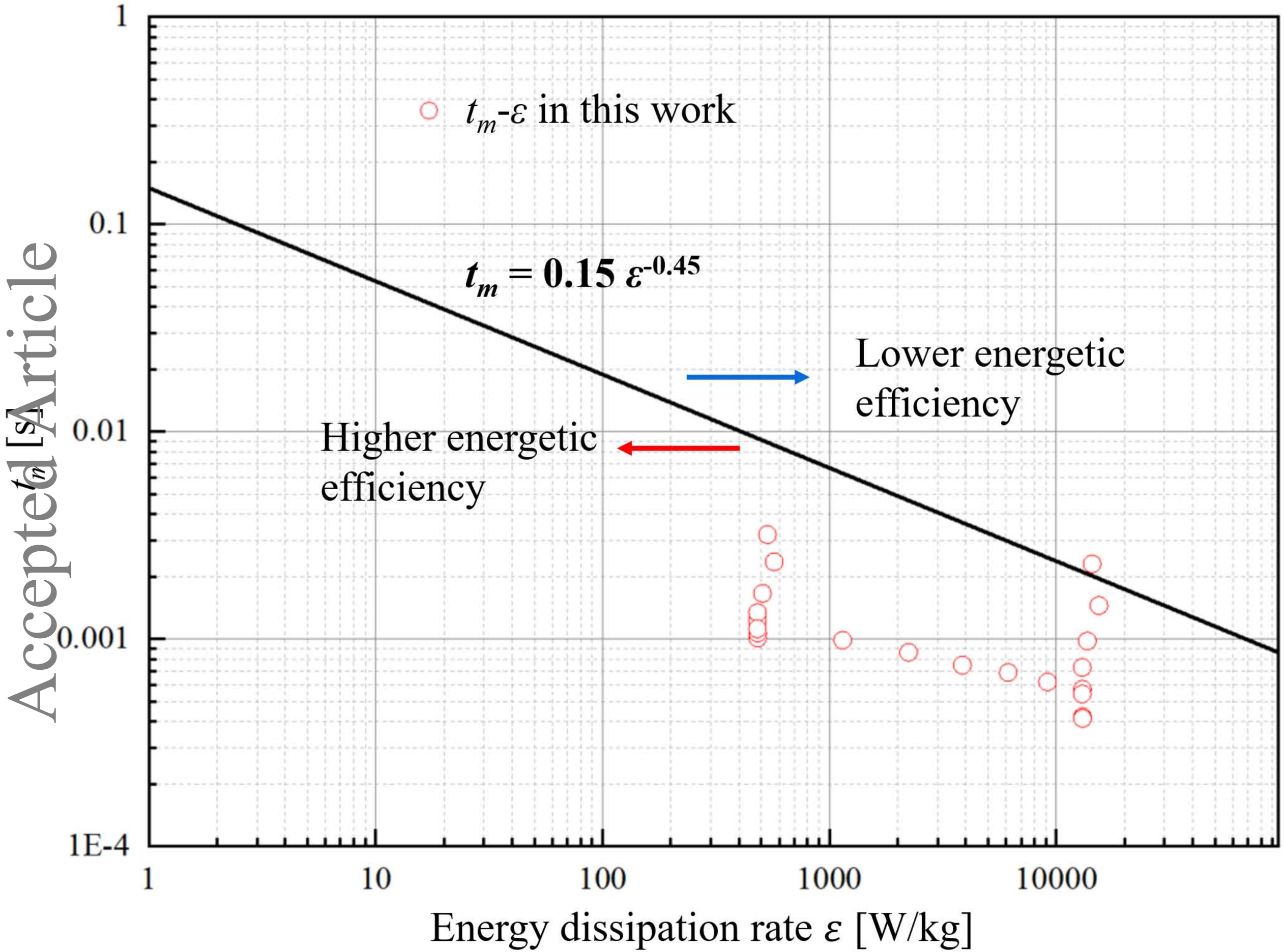
t_m-ε in this work
$t_m = 0.15\ \varepsilon^{-0.45}$
Lower energetic efficiency
Higher energetic efficiency
Accepted t_m [s]
1
0.1
0.01
0.001
1E-4
1
10
100
1000
10000
Energy dissipation rate ε [W/kg]